Structural Phase Transition and Material Properties of Few-Layer Monochalcogenides

Mehrshad Mehboudi,[1] Benjamin M. Fregoso,[2] Yurong Yang,[1] Wenjuan Zhu,[3] Arend van der Zande,[4]
Jaime Ferrer,[5] L. Bellaiche,[1] Pradeep Kumar,[1] and Salvador Barraza-Lopez[1,*]

[1]*Department of Physics, University of Arkansas, Fayetteville, Arkansas 72701, USA*
[2]*Department of Physics, University of California, Berkeley, California 94720, USA*
[3]*Department of Electrical and Computer Engineering, University of Illinois at Urbana-Champaign,
Urbana, Illinois 61801, USA*
[4]*Department of Mechanical Science and Engineering, University of Illinois at Urbana-Champaign,
Urbana, Illinois 61801, USA*
[5]*Departamento de Física, Universidad de Oviedo, 33007 Oviedo, Spain*
(Received 18 January 2016; revised manuscript received 25 October 2016; published 9 December 2016)

GeSe and SnSe monochalcogenide monolayers and bilayers undergo a two-dimensional phase transition from a rectangular unit cell to a square unit cell at a critical temperature T_c well below the melting point. Its consequences on material properties are studied within the framework of Car-Parrinello molecular dynamics and density-functional theory. No in-gap states develop as the structural transition takes place, so that these phase-change materials remain semiconducting below and above T_c. As the in-plane lattice transforms from a rectangle into a square at T_c, the electronic, spin, optical, and piezoelectric properties dramatically depart from earlier predictions. Indeed, the Y and X points in the Brillouin zone become effectively equivalent at T_c, leading to a symmetric electronic structure. The spin polarization at the conduction valley edge vanishes, and the hole conductivity must display an anomalous thermal increase at T_c. The linear optical absorption band edge must change its polarization as well, making this structural and electronic evolution verifiable by optical means. Much excitement is drawn by theoretical predictions of giant piezoelectricity and ferroelectricity in these materials, and we estimate a pyroelectric response of about 3×10^{-12} C/K m here. These results uncover the fundamental role of temperature as a control knob for the physical properties of few-layer group-IV monochalcogenides.

Few-layer group-IV monochalcogenides are semiconductors [1–7] with a structure similar to that of black phosphorus that exhibit a giant piezoelectric response in monolayer (ML) samples according to theory [5,8]. The fourfold degeneracy of their structural ground state first predicted by us in the past [9] leads to ferroelectricity [9–11]. These materials bring the concept of two-dimensional (2D) valleytronics on materials with reduced structural symmetries [12] closer to reality too [13]. Ferroelectrics must also exhibit a pyroelectric response, yet no theoretical description of this process has been provided for these 2D materials as of now.

It remains unknown whether these materials undergo a complete degradation when exposed to air at the few-layer limit. Nevertheless, theory tells us that these monolayers host two-dimensional piezoelectricity, ferroelectricity, and a valley physics that is addressable with linearly polarized light. The previous qualities do not exist simultaneously in any other known 2D atomic phase and justify additional theoretical and experimental studies. Adding to this list of properties, here we show that a structural transition taking place at finite temperature T modifies their band structure and hence their hole transport and optical properties, and induces a pyroelectric response. Realizing this host of

theoretical predictions requires thermally controllable experimental studies of few-layer monochalcogenides in an inert atmosphere.

Theoretical results based on density-functional theory in Refs. [1–7,10,11,13] correspond to structures at $T < T_c$ displayed in Fig. 1(a), and belong at the far left on the structure versus T plots in Figs. 1(c)–1(f). We performed Car-Parrinello molecular dynamics (MD) calculations at finite T [14–18] on 8×8 ML and AB-stacked bilayer (BL) supercells containing up to 512 atoms, with pseudopotentials and basis sets carefully validated [19], that led to the structural evolution at finite T presented in Figs. 1(c)–1(f). In order to focus on the results, thorough descriptions of methods, as well as the full time evolution of the instantaneous T, total energy E, in-plane stress, and order parameters at selected target temperatures are provided as Supplemental Material [20], Sec. I.

In Fig. 1(a) we illustrate a 2D structural transition whereby a rectangular unit cell with threefold coordinated atoms at $T < T_c$ turns into a square unit cell with fivefold coordinated atoms at $T \geq T_c$. The transition is captured in Figs. 1(c)–1(f) by the thermal evolution of the structural order parameters shown in Fig. 1(b) that include (i) lattice constants a_1 and a_2, obtained in four (eight) inequivalent
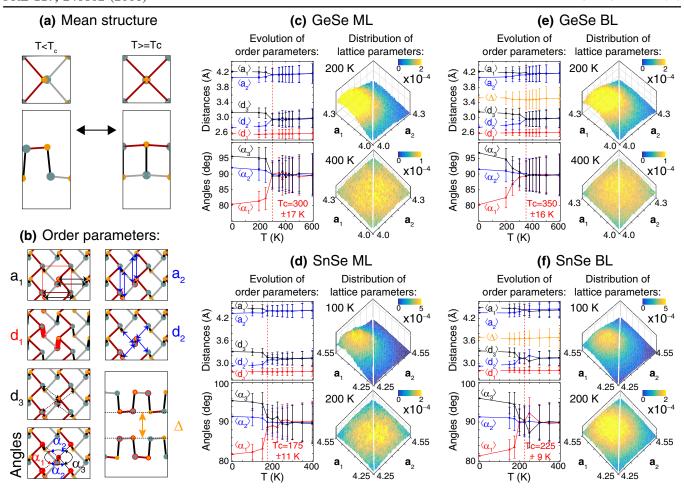
FIG. 1.   (a) Schematic depiction of the structural transition. (b) Structural order parameters highlighting the transition. (c)–(f) Left: thermal averages for the order parameters provided in (b) as a function of T for GeSe and SnSe MLs and BLs. T_c is reached when $\langle a_1 \rangle = \langle a_2 \rangle$, $\langle d_2 \rangle = \langle d_3 \rangle$, and $\langle \alpha_1 \rangle = \langle \alpha_2 \rangle = \langle \alpha_3 \rangle$. The average distance among layers $\langle \Delta \rangle$ for BLs is shown too. Right: the distribution of lattice parameters a_1 and a_2 dramatically highlights the fluctuations leading to the error bars on the subplots on the left. The line $a_1 = a_2$ is shown in white.

ways in MLs (BLs) at any given unit cell, (ii) interatomic distances up to third nearest neighbors (d_1, d_2, and d_3), and (iii) angles subtended among a given atom and its second-nearest neighbors (α_3), third-nearest neighbors (α_1), and second- and third-nearest neighbor (α_2).

The time autocorrelation of order parameters a_1 and a_2—a measure of the time scale of structural fluctuations—vanishes within 800 fs (Fig. 5 of Ref. [20]). Ensemble averages obtained from trajectories over 15 000 fs after thermal equilibration are reported in Figs. 1(c)–1(f) for $\langle a_1 \rangle$, $\langle a_2 \rangle$, $\langle d_i \rangle$, and $\langle \alpha_i \rangle$ ($i = 1, 3$).

Sudden changes of structural order parameters signal the transition temperature T_c: $\langle a_1 \rangle / \langle a_2 \rangle$ is greater than 1 at $T = 0$ K, and the transition is signaled by a rapid decay into $\langle a_1 \rangle / \langle a_2 \rangle = 1$. This ratio of lattice parameters decreases with increasing atomic number, so that SnSe MLs are expected to have a smaller T_c than GeSe MLs [9]. Additional signatures of the transition are the coalescence of d_2 and d_3 into a single value, and the coalescence of

in-plane angles defined in Fig. 1(b) toward 90°. As seen in Fig. 1, the transition occurs at $T_c = 175 \pm 11$ K for SnSe MLs and at a higher temperature of 350 ± 16 K for GeSe MLs. It is interesting to note that the square unit cell—corresponding to a point of unstable equilibrium at $T = 0$ K [9,21]—becomes, on average, the preferred structure at T_c.

Now, $\langle a_1 \rangle / \langle a_2 \rangle$ is known to increase with the number of layers for a given layered monochalcogenide as well [4] and, accordingly, one should expect an increase of T_c for a given material in going from MLs to BLs. Within the temperature resolution of 25 K employed in our calculations, we see a 50 K increase of T_c in going from MLs to BLs. Such an increase makes our results consistent with experiments on bulk SnSe, where T_c is of the order of 800 K [21–24] (MD simulations of bulk samples require the inclusion of four monolayers and are out of our reach). The structural change discussed in this and in the previous paragraph should be experimentally observable with x-ray diffraction (XRD) techniques.
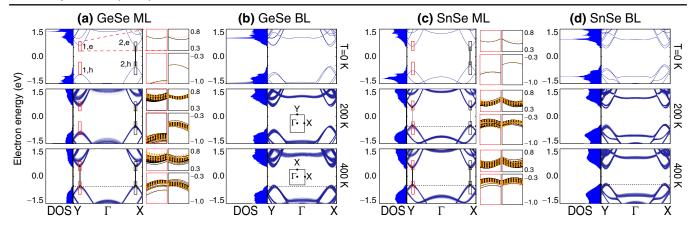
FIG. 2.   Electronic DOS and band structures for $t_i = 5000 + 100i$ fs ($i = 1, 2, 3, …, 150$) for (a) a GeSe ML, (b) a GeSe BL, (c) a SnSe ML, and (d) a SnSe BL at 0, 200, and 400 K. The zero energy was set at the midgap. The DOS and band structures become broader with increasing T, but no in-gap states are seen in the DOS or the band structures despite fluctuations. The X and Y points are inequivalent for $T < T_c$ and become equivalent for $T \geq T_c$ as $a_1 = a_2$. The thermal dependence of the hole conductivity should display an anomalous behavior when valleys $1, h$ and $2, h$ align at T_c.

We note that a melting transition would be signaled by an isotropic increase of interatomic distances $\langle d_1 \rangle$, $\langle d_2 \rangle$, and $\langle d_3 \rangle$. But the mean (intersublayer) distance $\langle d_1 \rangle$ in Figs. 1(c)–1(f) remains constant through the transition, displaying smaller fluctuations than (intrasublayer) distances $\langle d_2 \rangle$ and $\langle d_3 \rangle$, so that individual MLs retain their 2D character through the transition. An additional (geometrical) argument for the 2D character of the transition can be made from $\langle \alpha_i \rangle$ ($i = 1, 2, 3$) too: $\langle \alpha_1 \rangle + 2\langle \alpha_2 \rangle + \langle \alpha_3 \rangle$ add up to 2π. The angle defect, defined as $2\pi - (\langle \alpha_1 \rangle + 2\langle \alpha_2 \rangle + \langle \alpha_3 \rangle)$, is equal to zero only on a planar structure [25].

Structural degeneracies lead to an anharmonic elastic energy profile [9] and hence to soft ("floppy") phonon modes in monochalcogenide layered materials [21,23,24]; anharmonicity makes it relevant to discuss fluctuations. The distribution of lattice parameters shown at the right subplots in Figs. 1(c)–1(f) for increasing T has a mean value converging towards the (white) diagonal line $a_1 = a_2$ at T_c, which is consistent with a displacive transition [21]. The maximum height of the distribution decays sharply nevertheless, making the distribution extremely broad as the temperature rises. This broad distribution sets the error bar on $\langle a_1 \rangle$ and $\langle a_2 \rangle$ and is a signature of atomistic fluctuations (disorder). Excursions of a_1 and a_2 towards the right of the white $a_1 = a_2$ line gain a finite probability with increasing temperature, and a_1 and a_2 have a rather homogeneous distribution at T_c. Considering these fluctuations, the material properties to be discussed next were evenly sampled out of 150 individual frames at times $t_i = 5000 + 100i$ fs ($i = 1, 2, 3, …, 150$).

These materials remain semiconducting through the transition: the electronic DOS obtained on instantaneous supercells at times t_i in Fig. 2 shows a well-defined band gap for T below and above T_c (details of the DOS calculations are disclosed in Ref. [20]). The band gaps

in Fig. 2—whose magnitudes are explicitly reported in Table I of Ref. [20]—change by about 200 meV at 400 K with respect to their values at 0 K. The DOS has two additional features: (i) the sharpest peaks at 0 K become blurred at increasing T and (ii) shallow DOS pockets around the valence-band maximum for $T < T_c$.

The band structures in Fig. 2 were obtained from instantaneous unit cells built from average lattice and basis vectors at times t_i defined above. The width of these bands is another experimentally observable indicator of structural fluctuations that must be visible in angle-resolved photoemission spectroscopy data. The sharp peaks in the DOS at 0 K correspond to relatively flat bands located around the Γ point whose energy location fluctuates with increasing T, thus making these peaks shallower. A band unfolding scheme [26–29] confirms these findings.

Two-dimensional materials with reduced structural symmetries originate a novel paradigm in valleytronics in which the crystal momentum labels the individual valleys one to one [12]. In SnSe and GeSe MLs and BLs, the shallow DOS pocket at 0 K ($\langle a_1 \rangle > \langle a_2 \rangle$) corresponds to a hole valley $(2, h)$ located along the $\Gamma - X$ line in Fig. 2 [1,2,4] that lies at a higher energy when contrasted to the hole valley along the $\Gamma - Y$ line $(1, h)$.

The band structure insets in Fig. 2 show the effect of T on the valley spin polarization that arises due to spin-orbit coupling [30]. The spin polarization in these insets becomes drastically degraded at T_c because the spin-up (solid black) and spin-down (dashed yellow) bands become broader and closer together. For this reason, the remaining results in this Letter will neglect the effect of spin-orbit coupling. (*AB* BLs have zero spin polarizations at individual valleys due to inversion symmetry.)

As shown thus far, MLs and BLs increase their structural symmetry as T_c is approached from below (Fig. 1). This
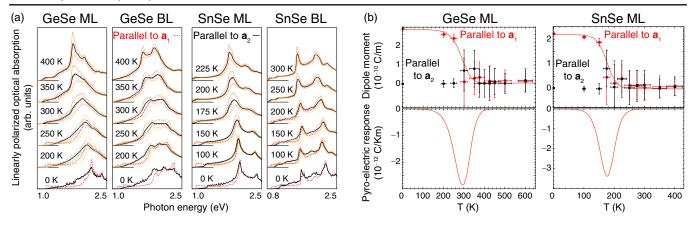
FIG. 3. (a) Linearly polarized optical absorption spectra. The gray and dashed orange lines are error bars. (b) Upper subplots: thermal evolution of the electric dipole moment per unit cell p. Lower subplot: pyroelectric response dp/dT.

means that the X and Y points in reciprocal space—which were inequivalent for $T < T_c$—become equivalent for $T \geq T_c$ as $\langle a_1 \rangle = \langle a_2 \rangle$. As T_c is reached, the hole valley along the $\Gamma - Y$ direction rises up to align with the valley located along the $\Gamma - X$ line (Fig. 2). One valley contributes to the hole conductivity at the band edge for $T < T_c$, while two valleys contribute at $T \geq T_c$, giving rise to an anomalous thermal dependence of the hole conductivity at $T = T_c$ that should be visible in standard transport measurements of gated or hole-doped samples.

As seen in Fig. 3(a), crystal momentum couples to the orientation of adsorbed linearly polarized light [13]. But the induced equivalence among the X and Y points for $T \geq T_c$ makes the optical adsorption band edges for horizontally and vertically polarized light identical, causing the band edge to become polarized at 45°, which then represents an additional, optical signature of the structural transition.

The binary composition of MLs and the asymmetry upon inversion about an axis parallel to $\mathbf{a}_2$ originates a net electric dipole p along the longest lattice vector $\mathbf{a}_1$ [3], resulting in a piezoelectric response at 0 K [5,8]. But as α_1, α_2, and α_3 fluctuate [Figs. 1(c)–1(f)], the orientation of these dipoles randomizes at T_c, turning the net electric dipole moment to zero. This hypothesis is demonstrated in Fig. 3(b) by averaging the mean electric dipole moment [31–35] over times t_i at a given T in instantaneous average unit cells (Sec. VI of Ref. [20]).

The three salient features of ferroelectrics are (i) piezoelectricity, (ii) ferroelectricity, and (iii) pyroelectricity. The abrupt decay of p around T_c was fitted to sigmoidal functions, whose temperature derivative dp/dT is the pyroelectric response given in the lower subplots in Fig. 3(b). The pyroelectricity hereby predicted may very well be a first within the field of 2D atomic materials.

To conclude, we predict a structural transition in MLs and AB BLs of GeSe and SnSe. The transition should be observable in mean values of lattice parameters and (in-plane) distances and angles among second and third nearest neighbors (XRD). These materials remain semiconductors through the transition, which should also be observable through angle-resolved photoemission spectroscopy, hole conductivity, and optical absorption measurements. We contributed the pyroelectric response of GeSe and SnSe MLs as well. These theoretical results may motivate and guide future experimental work in these few-layer materials with detailed thermal control and performed in an inert atmosphere.

*sbarraza@uark.edu

[1] G. A. Tritsaris, B. D. Malone, and E. Kaxiras, J. Appl. Phys. **113**, 233507 (2013).

[2] A. K. Singh and R. G. Hennig, Appl. Phys. Lett. **105**, 042103 (2014).

[3] Z. Zhu, J. Guan, D. Liu, and D. Tománek, ACS Nano **9**, 8284 (2015).

[4] L. C. Gomes and A. Carvalho, Phys. Rev. B **92**, 085406 (2015).

[5] R. Fei, W. Li, J. Li, and L. Yang, Appl. Phys. Lett. **107**, 173104 (2015).

[6] A. M. Cook, B. M. Fregoso, F. de Juan, and J. E. Moore, arXiv:1507.08677.

[7] T. Morimoto and N. Nagaosa, Phys. Rev. B **94**, 035117 (2016).

[8] L. C. Gomes, A. Carvalho, and A. H. Castro Neto, Phys. Rev. B **92**, 214103 (2015).

[9] M. Mehboudi, A. M. Dorio, W. Zhu, A. van der Zande, H. O. H. Churchill, A. A. Pacheco-Sanjuan, E. O. Harriss, P. Kumar, and S. Barraza-Lopez, Nano Lett. **16**, 1704 (2016).

[10] M. Wu and X. Zeng, Nano Lett. **16**, 3236 (2016).

[11] H. Wang and X. Quian, arXiv:1606.04522.

[12] P. Rivero, J.-A. Yan, V. M. García-Suárez, J. Ferrer, and S. Barraza-Lopez, Phys. Rev. B **90**, 241408 (2014).

[13] A. S. Rodin, L. C. Gomes, A. Carvalho, and A. H. Castro Neto, Phys. Rev. B **93**, 045431 (2016).

[14] J. M. Soler, E. Artacho, J. D. Gale, A. Garcia, J. Junquera, P. Ordejon, and D. Sanchez-Portal, J. Phys. Condens. Matter **14**, 2745 (2002).

[15] R. Car and M. Parrinello, Phys. Rev. Lett. **55**, 2471 (1985).

[16] M. Parrinello and A. Rahman, Phys. Rev. Lett. **45**, 1196 (1980).

[17] J. Junquera, O. Paz, D. Sánchez-Portal, and E. Artacho, Phys. Rev. B **64**, 235111 (2001).

[18] K. Berland and P. Hyldgaard, Phys. Rev. B **89**, 035412 (2014).

[19] P. Rivero, V. M. Garcia-Suarez, D. Pereniguez, K. Utt, Y. Yang, L. Bellaiche, K. Park, J. Ferrer, and S. Barraza-Lopez, Comput. Mater. Sci. **98**, 372 (2015).

[20] See Supplemental Material at http://link.aps.org/supplemental/10.1103/PhysRevLett.117.246802 for thorough descriptions of technical details.

[21] C. W. Li, J. Hong, A. F. May, D. Bansal, S. Chi, T. Hong, G. Ehlers, and O. Delaire, Nat. Phys. **11**, 1063 (2015).

[22] T. Chattopadhyay, J. Pannetier, and H. V. Schnering, J. Phys. Chem. Solids **47**, 879 (1986).

[23] L.-D. Zhao, S.-H. Lo, Y. Zhang, H. Sun, G. Tan, C. Uher, C. Wolverton, V. P. Dravid, and M. G. Kanatzidis, Nature (London) **508**, 373 (2014).

[24] J. P. Heremans, Nat. Phys. **11**, 990 (2015).

[25] A. P. Sanjuan, M. Mehboudi, E. Harriss, H. Terrones, and S. Barraza-Lopez, ACS Nano **8**, 1136 (2014).

[26] T. B. Boykin and G. Klimeck, Phys. Rev. B **71**, 115215 (2005).

[27] V. Popescu and A. Zunger, Phys. Rev. Lett. **104**, 236403 (2010).

[28] C.-C. Lee, Y. Yamada-Takamura, and T. Ozaki, J. Phys. Condens. Matter **25**, 345501 (2013).

[29] J. Ferrer, C. J. Lambert, V. M. Garcia-Suarez, D. Z. Manrique, D. Visontai, L. Oroszlany, R. Rodriguez-Ferradas, I. Grace, S. W. D. Bailey, K. Gillemot, H. Sadeghi, and L. A. Algharagholy, New J. Phys. **16**, 093029 (2014).

[30] L. Fernandez-Seivane, M. A. Oliveira, S. Sanvito, and J. Ferrer, J. Phys. Condens. Matter **18**, 7999 (2006).

[31] R. D. King-Smith and D. Vanderbilt, Phys. Rev. B **47**, 1651 (1993).

[32] G. Kresse and J. Furthmüller, Phys. Rev. B **54**, 11169 (1996).

[33] J. P. Perdew, K. Burke, and M. Ernzerhof, Phys. Rev. Lett. **77**, 3865 (1996).

[34] P. E. Blochl, Phys. Rev. B **50**, 17953 (1994).

[35] G. Kresse and D. Joubert, Phys. Rev. B **59**, 1758 (1999).